Pramana – J. Phys. (2022) 96:167
https://doi.org/10.1007/s12043-022-02397-w

Production and characterisation of ^{20,22}Ne targets

P M PRAJAPATI[1,2,3,*], R G PIZZONE[3], AKASH HINGU[4], S MUKHERJEE[4] and S V SURYANARAYANA[2]

[1]Department of Nuclear Physics, Institute of Physics, Slovak Academy of Sciences, 845 11, Bratislava, Slovak Republic
[2]Manipal Centre for Natural Sciences, Manipal Academy of Higher Education, Manipal 576 014, India
[3]INFN-Laboratori Nazionali del Sud, Via Santa Sofia 62, 95123 Catania, Italy
[4]Physics Department, Faculty of Science, M.S. University of Baroda, Vadodara 390 002, India
*Corresponding author. E-mail: pareshkumar.p@manipal.edu

MS received 18 March 2021; revised 17 March 2022; accepted 29 March 2022

Abstract. Targets of ^{20}Ne and ^{22}Ne nuclides were produced for nuclear astrophysics experiments by implanting them into tantalum backing material at the Ion Beam Centre (IBC), Helmholtz Zentrum Dresden Rossendorf (HZDR), Dresden. Each Ne nuclide was implanted alternatively at 30 keV and 50 keV. As significant sputtering of both neon and tantalum atoms occurs during implantation, the final neon depth profiles and areal densities of all four target types were analysed. Nuclear resonance analysis (NRA), Rutherford backscattering (RBS), elastic recoil detection analysis (ERDA) and proton-induced X-ray emission (PIXE) methods were used for detailed neon target analyses using the 6 MV Tandetron facility at the Advanced Technologies Research Institute of the Faculty of Materials Science and Technology in Trnava. Nuclear reactions ^{22}Ne(p, γ)^{23}Na at resonance energy (E_{res}) = 639 keV and ^{20}Ne(p, γ)^{21}Na at $E_{\mathrm{res}} = 1169$ keV were used for neon concentration depth profiling. The measured depth profiles were compared with the predictions given by the SRIM and the dynamic TRIDYN implantation simulations, which also consider the sputtering process. Impurity contamination and substrate roughness were checked by PIXE and ERDA measurements, respectively. The NRA technique was suitable for monitoring the target stability after one year of implantation.

Keywords. Neon implantation; ion beam analysis; depth profile; nuclear resonance analysis; ^{20}Ne; ^{22}Ne.

PACS Nos **24.10.-I; 26.50.+x**

1. Introduction

The neon–sodium cycle (Ne–Na cycle) plays a crucial role in hydrogen burning for synthesising elements between ^{20}Ne and ^{24}Mg [1] with important consequences on massive star nucleosynthesis. The sequence of reactions involved in this cycle is

$$^{20}\mathrm{Ne(p,\ }\gamma)^{21}\mathrm{Na}(\beta^{+}\nu)^{21}\mathrm{Ne(p,\ }\gamma)^{22}\mathrm{Na}(\beta^{+}\nu)\ ^{22}\mathrm{Ne(p,\ }\gamma)^{23}\mathrm{Na(p,\ }\alpha)^{20}\mathrm{Ne}. \quad (1)$$

Further, ^{22}Ne(α, n)^{25}Mg and ^{22}Ne(α, γ)^{26}Mg reactions have immense importance in determining the number of neutrons available for the astrophysical s-process, specifically in the case of massive stars. This process is responsible for producing elements heavier than iron using neutron captures and subsequent beta decays starting from lighter 'seed' nuclides. Such evidence is observed in the solar systems abundance pattern [2,3] and explains some of its features. Thus, there has been strong demand in the astrophysics community for the reaction rate measurement for the reactions mentioned earlier. Such nuclear input must be known in the stellar environment and at the corresponding energies (a few hundred keVs in such cases). Measurements at higher energies (1–6 MeV) are also required for different purposes [4,5].

Reactions between charged particles have a minimal cross-section over the energy range for stellar temperature, often of the order of nanobarns or picobarns. This is an apparent effect of the Coulomb penetration factor, which suppresses reaction cross-sections at lower energies [6]. It is necessary to use a high beam current (within the physical limit of target damage) to

Published online: 06 September 2022

compensate and maximise the reaction yield for direct reactions. Moreover, stable targets with a large number of nuclei (as allowed by the desired energy resolution) and a detection technique with high efficiency for direct measurements are suitable [7–9]. In our case, neon is available in gaseous form with two main isotopes, ^{20}Ne (90.48%) and ^{22}Ne (9.25%) [10]. Both are important for stellar nucleosynthesis, as discussed above.

Moreover, neon isotopes can play a crucial role also for the application of indirect methods for nuclear astrophysics (for instance, the Trojan Horse Method [11,12]). In particular, ^{20}Ne has been suggested to be used as a possible virtual source of ^{16}O to study ^{16}O + ^{16}O [13,14], which is very important for oxygen burning in massive star nucleosynthesis. A similar method was already applied to the essential ^{12}C + ^{12}C reaction with pioneering results [15].

If the target is available as an isotopically pure gas, windowless and supersonic-jet type has been used [16,17]. In other cases, solid targets must be used, which should be highly stable against high-intensity ion beams with minimum background reactions induced on the impurities in the target [4]. Using an isotope separator appears to be a reasonable means for producing isotopically enriched targets of various elements capable of withstanding high beam loads [7]. Several measurements used implanted neon targets [18–20] but did not provide detailed information on its characterisation. The detailed characterisation of the implanted targets is essential for precisely determining reaction rates and astrophysical factors as it gives accurate data of implantation, the depth profile of the target and trace impurities if any. It is also crucial to check the isotopic purity of the prepared ^{20}Ne- and ^{22}Ne-implanted targets and their possible contamination by other elements. For nuclear reaction studies of astrophysical interests, with a very low cross-section, the maximal suppression of side effects and disturbing signal background, as well as the long-term target stability, are crucial. Therefore, it is necessary to track any changes in Ne targets, namely changes in the quantity and depth profile of implanted neon atoms in the Ta substrate before, during and after 'astrophysical' measurements.

The present work aims to produce and characterise the isotopically pure implanted neon targets, namely, ^{20}Ne and ^{22}Ne. In this context, ^{20}Ne- and ^{22}Ne-implanted targets have been produced on tantalum backing using 200 kV ion implanter facility at IBC, HZDR, Rossendorf, Dresden at 30 and 50 keV alternatively. Four types of targets were prepared by isotopically pure ion implantation. The detailed characterisations of implanted neon targets were performed using the 6 MV Tandetron Facility at STU, Trnava. Standard NRA [21] and RBS [22] ion beam analytical methods were employed to study Ne depth profiles. The measured depth profiles were compared with the predictions given by SRIM [23,24] and the dynamic TRIDYN [25] implantation simulations, which consider the sputtering process. The impurity contamination and substrate roughness were checked by PIXE [26], ERDA [27] and SEM [28] measurements, respectively.

2. Experimental procedure

2.1 *Production of ^{20}Ne and ^{22}Ne targets*

Targets of ^{20}Ne and ^{22}Ne nuclides were prepared by implantation into 5 μm thick tantalum backing material. They were prepared by isotopically pure ^{20}Ne and ^{22}Ne ion implantations at IBC, HZDR using a 200 kV ion implanter (Danfysik A/S, Model 1090). Ion beams were extracted from a Ne plasma in an ion source using an extraction voltage of 30 kV, mass separated by a sector magnet and partially post-accelerated using an acceleration voltage of 20 kV to obtain ion energies of 30 keV and 50 keV, respectively. The ion beams were guided to the implantation endstation and raster-scanned across the samples using electrostatic plates ($f \sim 1$ kHz). The ion fluence was measured using four Faraday corner cups. All samples have been clamped on a liquid nitrogen cooling target to keep the sample temperature below $-$ 35°C during ion irradiation. The base pressure in the implantation chamber was less than 2×10^{-6} mbar.

2.2 *Characterisations of ^{20}Ne- and ^{22}Ne-implanted targets*

Ion beam analysis (IBA) methods [21] were used to characterise the prepared Ne targets. In particular, the Rutherford backscattering spectrometry (RBS), nuclear resonance analysis (NRA), proton-induced X-ray emission (PIXE), as well as elastic recoil detection analyses (ERDA) have been employed for detailed elemental analysis and, in some cases, related to depth distribution. Since each IBA method has its specific advantages, the most appropriate method was chosen for each observed parameter. The IBA was carried out in the laboratory of a 6 MV tandem ion accelerator at the Slovak University of Technology, situated in Trnava, Slovakia [29,30]. The analysis procedures used are discussed in detail below.

2.3 *PIXE, ERDA and RBS*

The information about the roughness of the implanted neon targets is important for subsequent IBAs evaluations. Thus, SEM images of the implanted neon targets were taken before starting detailed IBA. PIXE checked the presence of contamination by elements with atomic number $Z > 11$. A 2 MeV H^+ beam at a fluence of 20 μC was used for PIXE analysis at the normal sample incidence. The Canberra HPGe X-ray detector model GL0055% with 100 μm Mylar absorption foil in front of the detector situated at 45° to the sample normal direction was used for X-ray detection. The evaluation of measured spectra was done by the GUPIX code [31]. The presence of hydrogen in the surface region of the targets was checked by the ERDA method. In this method, a 3.25 MeV He^+ at 20° incident angle and 10° exit angle (30° scattering angle) with 12 μm thick Kapton absorption foil in front of the detector was used. Simultaneously with ERDA measurements, RBS spectra were also collected (170° backscattering angle). They were used for proton dose check during ERDA spectra acquisition and also for the first estimate of the implanted neon content in Ta targets. The presence of neon in the substrate was reflected by a decrease of the tantalum RBS signal. ERDA and RBS measurements were evaluated using the SIMNRA ver.7.01 [32] simulation program.

2.4 *NRA ^{20}Ne and ^{22}Ne depth profiling*

NRA method is an excellent tool to determine the thickness and uniformity of the implanted area using narrow resonance. The narrow resonant nuclear reaction ^{20}Ne(p, γ)^{21}Na, resonance energy (E_{res}) = 1169 keV [7] and ^{22}Ne(p, γ)^{23}Na reaction, resonance energy (E_{res}) = 639 keV [18], were utilised to measure ^{20}Ne and ^{22}Ne isotopes, respectively. In this way, the isotopic purity and depth concentration distribution of ^{20}Ne and ^{22}Ne targets were checked. The NRA extension setup based on the small target chamber located behind the IBA end station was used for resonant NRA measurements. To easily change the energy of the incident protons, the electrical potential of the chamber was controlled which could vary within ± 5 kV. For this reason, the NRA chamber was electrically isolated from both the beamline and the scintillation detector and connected to a regulated high voltage power supply. The sample was attached to the rear flange of the NRA chamber and the scintillation detector was positioned as close as possible behind the sample in the beam axes direction. Proton beam-induced gamma spectra were collected by 2″ × 2″ BrilLanCeTM 380 model 51S51 $LaBr_3$(Ce) scintillation detector, with an energy resolution of 32 keV (i.e. 2.4%) FWHM for 1.33 MeV, coupled to a Canberra DSA-LX™ Digital Signal Analyzer. Also, Canberra HPGe gamma detector model GC2518, with a relative efficiency of 26.4% and an energy resolution of 1.8 keV FWHM for 1.33 MeV was used for high-resolution gamma spectra control measurements.

The proton beam current during the analysis was 60 nA, the fluence 50 μC for each measuring point was monitored through RBS taken by a movable charged particle detector, of backscattering angle 175°, placed in the IBA chamber. The preset counts in the selected region of interest of Ta substrate RBS spectra controlled the predefined fluence for each single NRA measurement point. To cover the depth distribution in both the ^{20}Ne and ^{22}Ne cases, the proton energy was swept over the range of 25 keV. For each NRA measurement point, gamma radiation was recorded within the energy range up to 10 MeV. No peaks above 2.7 MeV energy in gamma spectra background were detected when the proton energy was below the corresponding resonant energy. This energy was set as the lower limit for counting the gamma radiation signal of the observed nuclear reaction contribution. For measuring ^{20}Ne (1169 keV resonance) and ^{22}Ne (639 keV resonance), the region of interest (ROI) of gamma yield from 2.7 to 5.0 MeV (ROI) and from 2.7 to 6.0 MeV (ROI) was considered, respectively as shown in figure 1. The gamma yield in the corresponding ROIs has been corrected for the gamma background signal and for measuring time variation. The stopping powers and the densities of the target sublayers predicted by the TRIDYN calculation have been applied to convert proton energy to the target depth scale. From the recorded resonant gamma yield dependence of the implanted neon targets, the ^{20}Ne and ^{22}Ne, concentration depth profiles in Ta substrate were evaluated. The NRA characterisation experiments were carried out immediately after the implanted targets were produced, after four months of their production and after a year. During each experiment, we observed the same trend of the depth profiles of all four implanted targets. There have been no such changes. If there is a change in depth profile, it might affect the stoichiometry of the implanted neon, which may affect the astrophysical measurement of interest.

3. SRIM and TRIDYN simulations

Two computer codes, a Monte Carlo simulation code (SRIM-2013) and a dynamic computer simulation using binary collision approximation (TRIDYN-2017), were

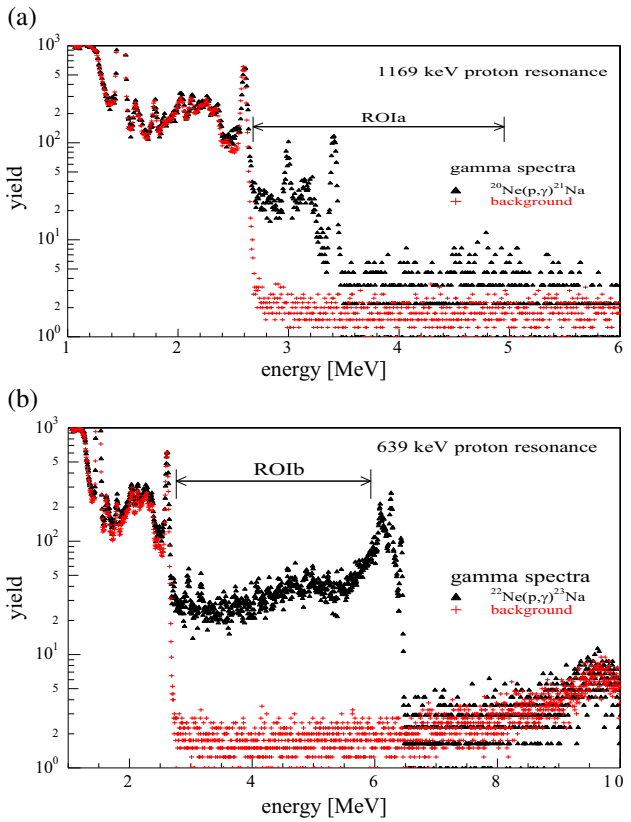

Figure 1. Gamma spectra recorded by the $LaBr_3$ scintillation detector during a depth profile measurement of (**a**) ^{20}Ne (1169 keV resonance) and (**b**) ^{22}Ne (639 keV resonance). In both cases, red colour represents the background gamma spectrum and black colour represents the gamma spectrum from resonant nuclear reactions. The regions of interest used for evaluation are indicated.

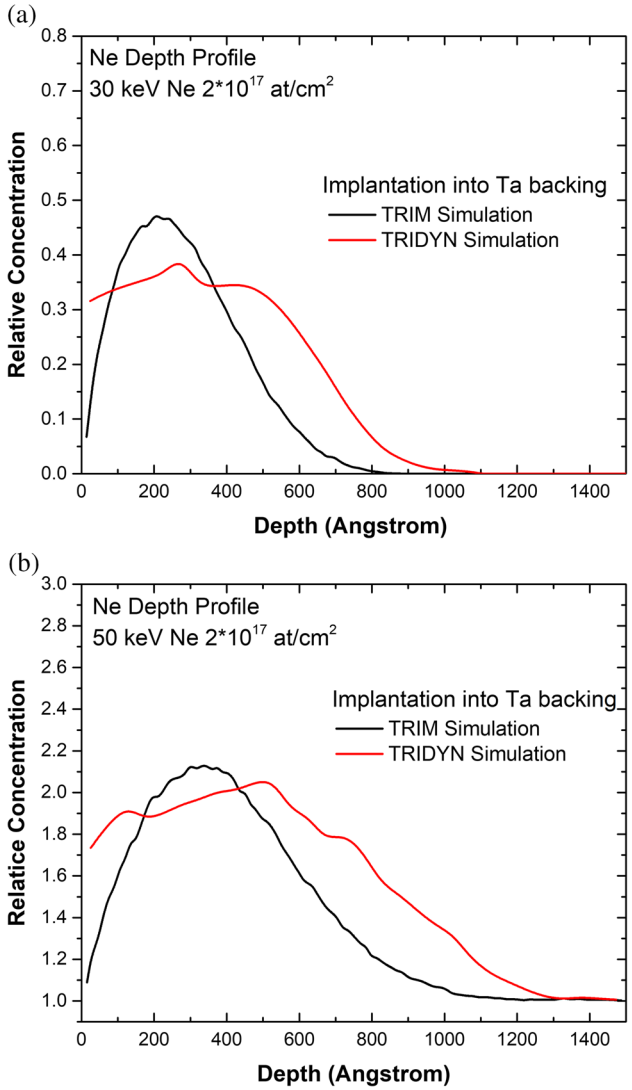

Figure 2. Depth profiles of Ne atoms implanted at energy 30 keV and 50 keV, simulated by SRIM2013 (static mode) and TRIDYN2017 (dynamic mode).

used to simulate the neon-implanted depth distribution. The standard SRIM considers the unaffected and unchanged target material for the entire calculation period. However, at a high fluence of low-energy neon implantation, intensive sputtering of target material occurs, which can affect the resulting neon depth profile and the total implanted dose. According to the SRIM calculations, one incident neon atom sputters an average of 1.6 atoms of the Ta substrate. However, TRIDYN considers dynamic changes in material composition upon irradiation due to the implantation of incident atoms, atomic relocation in the bulk and sputter erosion at the surface. TRIDYN should more realistically describe high-fluence implantation profiles. Since the isotopic effect on the simulated implanted depth profile was negligible, only the atomic simulation data are considered and presented. The simulated depth profiles of Ne atoms implanted at 30 and 50 keV energy by SRIM2013 (static mode) and TRIDYN2017 (dynamic mode) are shown in figure 2.

4. Results and discussion

As the backing material for ^{20}Ne and ^{22}Ne implantation, the 5 μm thick high-purity tantalum sheet was used. Pure Ta sheets were implanted, and we used rough/original surface. We did not perform any experiment to make the surface smooth to avoid possible contamination of the substrate material. This information indicates that the subsequent IBA analysis should be performed preferably at the normal incidence of the analysing ion beam to the target surface. If possible, the glancing geometry should be avoided. This information was considered during the subsequent IBA analysis. PIXE analysis did not reveal any contamination by elements with atomic number $Z > 11$ in a concentration over 10 atomic ppm limit. ERDA analysis showed that about 100 nm target

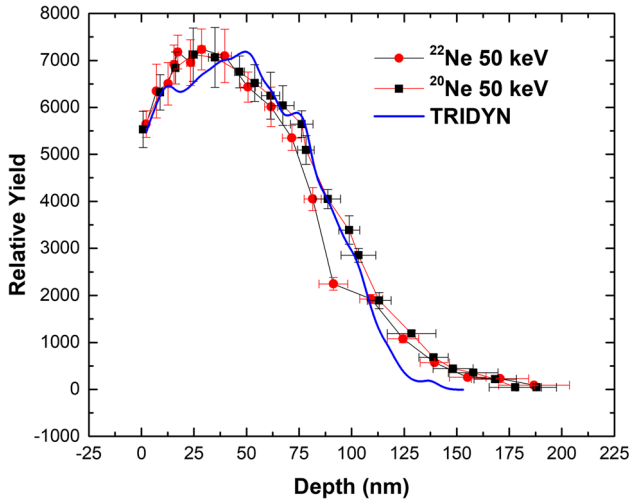

Figure 3. The implanted neon depth profile along with TRIDYN-simulated results at 50 keV.

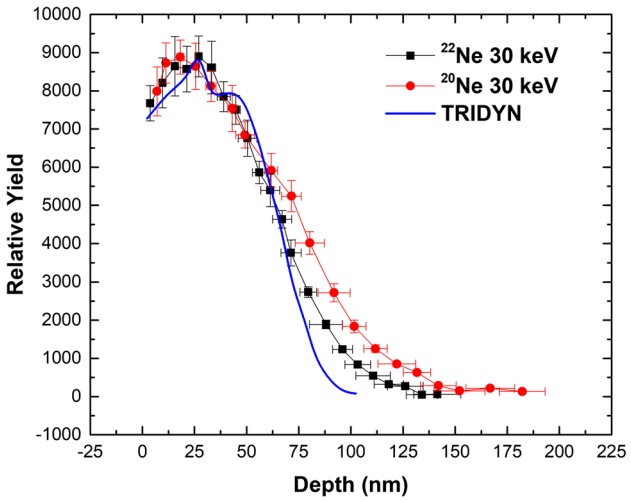

Figure 4. The implanted neon depth profile along with TRIDYN-simulated results at 30 keV.

surface layer contains up to 1×10^{17} at/cm^2 of hydrogen. The specific hydrogen content varied in different samples and probably depended on the history of sample maintenance. Estimates of the neon content from RBS spectra confirmed neon-implanted fluence of 2×10^{17} at/cm^2 within an uncertainty of 15%.

The comparison of the static SRIM/TRIM and the dynamic TRIDYN calculations of the concentration profiles reveal a difference in the surface area (sputtering effect) and in the range (target composition, recoil, diffusion effects) when taking into account the change in sample composition during the calculation as shown in figure 2. After 1×10^{17} at/cm^2 fluence neon implantation, the neon content in the surface target layer can reach up to 30%. Such high concentration may pose a risk in terms of the long-term stability of Ne content in the targets. From the comparison with the measured values given below, TRIDYN gives more realistic outcomes. An implantation profile indicates the Bragg curve reaching a certain depth depending on the implantation energy. Implantation with two different energies leads to a little different depth profile and increases the total number of atoms implanted beyond the saturation value of a single implantation. The implanted neon depth profile along with TRIDYN-simulated results are plotted in figures 3 and 4. Figure 3 shows that there is a good agreement of 50 keV-implanted ^{20}Ne, ^{22}Ne and of 30 keV-implanted ^{20}Ne measured depth profiles with the TRIDYN theoretical ones as shown in figure 4. Good agreement can be seen, especially from the surface to the depth where the neon concentration is roughly 1/2 of its maximum value. Then, at a greater depth, the measured tail reaches deeper than the theoretical prediction. However, in the case of 30 keV-implanted ^{22}Ne, the measured tail goes deeper than TRIDYN-simulated and then the ^{20}Ne measured profile. It may be due to the higher fluence radiation dose. This discrepancy was also confirmed by repeated NRA measurements.

Further, NRA measurement repeated after a year showed perfect match with the first results, indicating good time stability of the prepared neon samples. The results of neon target analyses have demonstrated the applicability of the presented ion beam analytical methods for its quality and stability monitoring. In particular, it is also suitable to track possible changes in neon content in Ta targets during and after loading of high doses during future astrophysical experiments.

5. Conclusions

Targets of ^{20,22}Ne nuclides have been produced for nuclear astrophysics experiments by implantation into Ta backing materials at 30 and 50 keV. The properties of the targets were studied using different IBA methods. It is found that the implantation technique provides a suitable means to produce isotopically enriched targets capable of long-lasting irradiation. It is observed that PIXE analysis did not reveal any contamination by elements with atomic number $Z > 11$, whereas ERDA analysis provides important information about hydrogen content on the implanted target surface layer. Thus, it is evident that the implanted neon target has a significant amount of hydrogen contamination, which should be taken care of and considered during the astrophysical measurements in future. Comparing the static SRIM and the dynamic TRIDYN calculations of the concentration profiles reveal a difference in the surface area. TRIDYN considers dynamic changes in material composition upon irradiation due to the implantation of

incident atoms due to atomic relocation in bulk and sputter erosion at the surface. It is found that TRIDYN describes high-fluence neon implantation depth profiles more accurately at 50 keV. The repeated NRA measurement after one year showed a perfect match with initial results, reflecting the excellent time stability of the implanted neon targets.

Acknowledgements

This work was supported by the grant received from Programme SASPRO No. 0098/01/01, which is co-funded by the European Commission under the scheme 'Co-financing of regional, national and international programs (COFUND)', which is part of the Marie Curie Action of the EU 7th Framework Programme, under Grant Agreement No. REA 609427: SASPRO/Mobility Programme of the Slovak Academy of Sciences. The authors are thankful to R Boettger of HZDR, Rossendorf, for providing the experimental facility for ion implantation. Special thanks are also due to D Vana, J Dobrovodsky of Slovak Technical University, Trnava, for providing smooth beam time for the characterisation of the implanted neon targets. One of the authors, PMP, is grateful to M Venhart, Institute of Physics, Slovak Academy of Sciences, for valuable discussions and suggestions.

References

[1] J Marion and W Fowler, *Ap. J.* **125**, 221 (1957)
[2] E M Burbidge *et al*, *Rev. Mod. Phys.* **29**, 547 (1957)
[3] F Kappeler *et al*, *Rev. Mod. Phys.* **83**, 157 (2011)
[4] W A Fowler, *Rev. Mod. Phys.* **56**, 149 (1984)
[5] C Rolfs, H P Trautvetter and W S Rodney, *Rep. Progr. Phys.* **50**, 233 (1987)
[6] H Lee, J Gorres, H W Becker, E Stech, E Strandberg and M Wiescher, *Nucl. Instrum. Methods Phys. Res. B* **267**, 3539 (2009)
[7] S Seuthe *et al*, *Nucl. Instrum. Methods Phys. Res. A* **260**, 33 (1987)
[8] E Selin, S Arnell and O Almén, *Nucl. Instrum. Methods* **56**, 218 (1967)
[9] J Keinonen, M Riihonen and A Anttila, *Phys. Rev. C* **15**, 579 (1977)
[10] NuDat (BNL, USA), www.nndc.bnl.gov/nudat2/
[11] A Tumino, C Bertulani, M L Cognata, L Lamia, R G Pizzone, S Romano and S Typel, *Annu. Rev. Nucl. Part. Sci.* **71**, 345 (2021)
[12] C Spitaleri, M La Cognata, L Lamia, R G Pizzone and A Tumino, *Eur. Phys. J. A* **55**, 161 (2019)
[13] S Hayakawa *et al*, *EPJ Web of Conferences* **117**, 09013 (2016)
[14] R G Pizzone *et al*, *Eur. Phys. J. A* **56**, 199 (2020)
[15] A Tumino *et al*, *Nature* **557**, 687 (2018)
[16] C Rolfs, J Górres, K U Kettner, H Lorenz-Wirzba, P Schmalbrock, H P Trautvetter and W Verhoeven, *Nucl. Instrum. Methods* **157**, 19 (1978)
[17] H W Becker, L Buchmann, J Gbrres, K U Kettner, H Kräiwmkel, C Rolfs, P Schmalbrock, H P Trautvetter and A Vlieks, *Nucl. Instrum. Methods* **198**, 277 (1982)
[18] R Depalo *et al*, *Phys. Rev. C* **92**, 045807 (2015)
[19] S Lyons *et al*, *Phys. Rev. C* **97**, 065802 (2018)
[20] P R Wren and R W Kavanagh, *Phys. Rev. C* **62**, 055805 (2000)
[21] M Wilde and K Fukutani, Nuclear reaction analysis, in: *Compendium of surface and interface analysis* (Springer, 2018) pp. 405–411
[22] L J Van I Jzendoorn, M J A de Voigt and J W Niemantsverdriet, *React. Kinet. Catal. Lett.* **50**, 131 (1993)
[23] J F Ziegler, *Nucl. Instrum. Methods Phys. Res. B* **136–138**, 141 (1998)
[24] J F Ziegler, M D Ziegler and J P Biersak, *Nucl. Instrum. Methods Phys. Res. B* **268**, 1818 (2010)
[25] W Möller and W Eckstein, *Nucl. Instrum. Methods Phys. Res. B* **2**, 814 (1984)
[26] W Maenhaut, *Nucl. Instrum. Methods Phys. Res. B* **49**, 518 (1990)
[27] M Nastasi, J W Mayer and Y Wang, *Ion beam analysis – Fundamental and applications* (CRC Press, 2014)
[28] A L Vasiliev, M V Kovalchuk and E B Yatsishina, *Cryst. Rep.* **61**, 873 (2016)
[29] P Noga, J Dobrovodský, D Vaňa, M Beňo, A Závacká, M Muška, R Halgaš, S Minárik and R Riedlmajer, *Nucl. Instrum. Methods Phys. Res. B* **409**, 264 (2017)
[30] J Dobrovodský *et al*, *IOP Conf. Ser.: Mater. Sci. Eng.* **465**, 012002 (2019)
[31] J L Campbell *et al*, *Nucl. Instrum. Methods Phys. Res. B* **499**, 77 (2021)
[32] M Mayer, *Nucl. Instrum. Methods Phys. Res. B* **194**, 177 (2002)